

VOLUME 41, 2020

JOURNAL OF DISPERSION SCIENCE AND TECHNOLOGY



INCLUDED IN THIS ONLINE EDITION:

AN INDEX IS



Taylor & Francis
Taylor & Francis Group



Journal

Journal of Dispersion Science and Technology >

This journal



Editorial board

Editor-in-Chief

Orlando Rojas

Professor and Canada Excellence Research Chair
Chemical & Biological Engineering,
The University of British Columbia,
2360 East Mall, Vancouver, BC Canada V6T 1Z3
Email: orlando.rojas@ubc.ca

Founding Editors

Stig E. Friberg (deceased)**Dr. Paul Becher (deceased)**

Editors Emeriti

John Texter - *Strider Research Corporation, 265 Clover St., Rochester, New York 14610, USA*

Regional Editors

Latin America: J.-L. Salager

Lab. FIRP, Ingeniería Química
Universidad de los Andes
Marida, Venezuela

Western Europe: Johan Sjöblom

Trondheim, Norway

Far East: R. Guo

Yangzhou University
Yangzhou, China

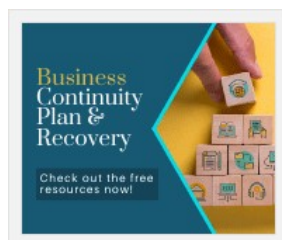
Australia: P. J. Scales

University of Melbourne
Victoria, Australia

Editorial Board

S.I. Anderson - *Technical University of Denmark, Lyngby, Denmark*
P. Claesson - *Royal Institute of Technology, Stockholm, Sweden*
D. Clausse - *University of Compiègne, Compiègne, France*
A. Dukhin - *Dispersion Technology, Bedford Hills, New York, USA*
S.S. Dukhin - *Goldens Bridge, New York, USA*
N. Garti - *Casali Institute for Applied Chemistry, Hebrew University, Jerusalem, Israel*
J. Genzer - *North Carolina State University, Raleigh, North Carolina, USA*
K. Holmberg - *Chalmers University of Technology, G teborg, Sweden*
I.B. Ivanov - *University of Sofia, Bulgaria*
G.J.M. Koper - *Technical University of Delft, The Netherlands*
P. Kumar - *EnDev Laboratories, Kannapolis, North Carolina, USA*
J. Laine - *Tampere University Hospital, Tampere, Finland*
G. Z. Li - *University of Shandong, Jinan, Shandong, China*
M. Lindgren - *Norwegian University of Science and Technology, Trondheim, Norway*
B. Lindman - *Lund University, Lund, Sweden*
O. Mullins - *Schlumberger Company, Houston, Texas, USA*
G. Oye - *Norwegian University of Science and Technology, Trondheim, Norway*
E. Pelizetti - *Universit de Torino, Torino, Italy*
R. Rodgers - *Florida State University, Tallahassee, Florida, USA*
Carlos Rodriguez-Abreu - *Institute for Advanced Chemistry, Catalonia, Spain*
E.D. Shchukin - *John Hopkins University, Baltimore, Maryland, USA*
P. Stenius - *Helsinki University of Technology, Helsinki, Finland*
M. Stocker - *SINTEF, Oslo, Norway*
C. Tsouris - *Oak Ridge National Laboratory, Oak Ridge, Tennessee, USA*
C.J. Van Oss - *State University of New York, Buffalo, New York, USA*
L. Wang - *Tsinghua University, Beijing, China*
D.T. Wasan - *Illinois Institute of Technology, Chicago, Illinois, USA*

[Sample our Engineering & Technology journals, sign in here to start your access, latest two full volumes FREE to you for 14 days](#)





Information for

[Authors](#)
[Editors](#)
[Librarians](#)
[Societies](#)

Open access

[Overview](#)
[Open journals](#)
[Open Select](#)
[Cogent OA](#)

Help and info

[Help & contact](#)
[Newsroom](#)
[Commercial services](#)
[All journals](#)
[Books](#)

Keep up to date

Register to receive personalised research and resources by email

 [Sign me up](#)



Copyright © 2020 Informa UK Limited [Privacy policy](#) [Cookies](#) [Terms & conditions](#) [Accessibility](#)

Registered in England & Wales No. 3099067
5 Howick Place | London | SW1P 1WG

About this journal



Sample Our
Engineering & Technology
journals

STAR INITIATIVE
Free article access
for authors from
the Global South

[Register for a voucher >](#)

Latest articles

Article

[Foam forming of fiber products: a review >](#)

Tuomo Hjelt et al.

Published online: 8 Mar 2021



Article

[Laboratory optimization of surfactant imbibition in high temperature and high salinity fractured reservoir >](#)

Renzhuo Wang et al.

Article

Fabrication of thermodynamically stable self-microemulsifying drug delivery system of resveratrol with enhanced solubility and chemical stability >

Sivaram Nallamolu et al.

Published online: 22 Feb 2021

Article

Parabolic effects of viscosity on dispersion and stability of millimeter-scale W1/O/W2 double droplets for ICF polymer shells >

Qiang Chen et al.

Published online: 22 Feb 2021


[View more>](#)

[See all volumes and issues](#)

	Volume 42, 2020-2021	Vol 41, 2020	Vol 40, 2019	Vol 39, 201 
---	-----------------------------	---------------------	---------------------	--

 Issue 
4 3 2 1



Browse by section (All) 



Display order (Default) 



Download citations



Download PDFs

Journal of Dispersion Science and Technology, Volume 42, Issue 3 (2021)

Articles

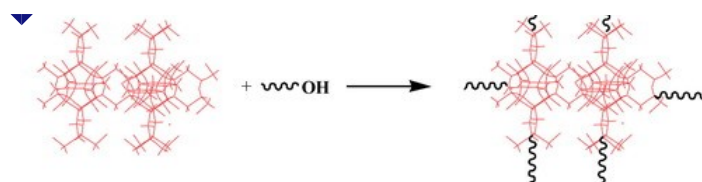


Article

[Organic–inorganic hybridized zeolite by polycardanol for ammonia-nitrogen adsorption >](#)

Chuan Gao, Ruobing Yu & Jian Huang

Pages: 319-327



93	0	0
Views	CrossRef citations	Altmetric

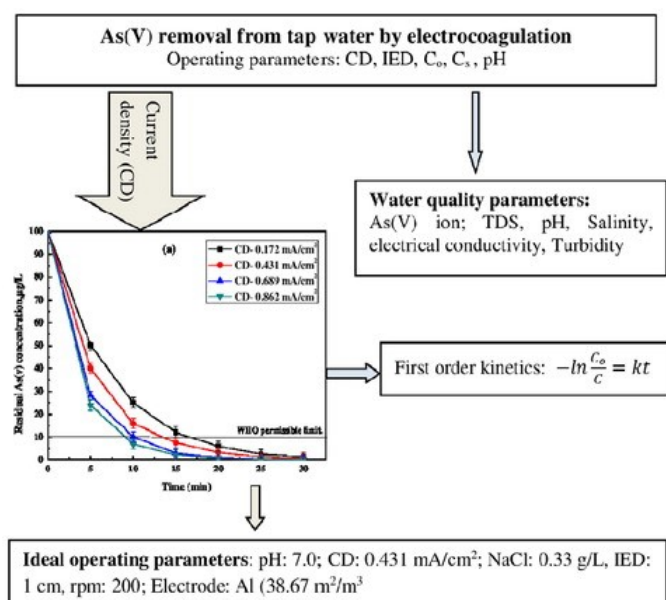
Article

[Arsenic removal from tap water by electrocoagulation: investigation of process parameters, kinetic analysis, and operating cost >](#)

Daisy Das & Barun Kumar Nandi

Pages: 328-337

Published online: 25 Oct 2019



129	4	0
Views	CrossRef citations	Altmetric

Article

[Formulation and characterization of water-based drilling fluids for gas hydrate reservoirs with efficient inhibition properties >](#)

Moumita Maiti, Ravi Ranjan, Ekta Chaturvedi, Ajoy Kumar Bhaumik & Ajay Mandal

Pages: 338-351

Published online: 30 Oct 2019

[Graphical abstract](#)

160	1	Altmetric
Views	CrossRef citations	

[Reservoir applicability and flooding effect of amphoteric ion crosslinked polymer solution >](#)

Jianbing Li, Wenxiang Wu, Liwei Niu, Mingxing Bai, Yue Zhang & Ying Jiang

Pages: 352-362

Published online: 04 Nov 2019[Graphical abstract](#)

43	0	Altmetric
Views	CrossRef citations	

Article

[Facile fabrication of versatile superhydrophobic coating for efficient oil/water separation >](#)

Taiheng Zhang, Shuai Wang, Jian Huang, Yingshan Jin, Guoqing Zhao, Chongyang Zhang, Caifeng Li, Jingang Yu, Yanlin Jia & Feipeng Jiao

Pages: 363-372

Published online: 07 Jul 2020[Graphical abstract](#)

112	0	Altmetric
Views	CrossRef citations	

Article

[Physicochemical and spectral evaluation of the interactional behavior of nicotinic acid \(vitamin B₃\) with mixed \[sodium deoxycholate \(bile salt\) + cetyltrimethylammonium bromide\] surfactants >](#)

Parampaul K. Banipal, Pallavi Sohal & Tarlok S. Banipal

Pages: 373-385

Published online: 16 Dec 2019[Graphical abstract](#)

59	0	Altmetric
Views	CrossRef citations	

Article

[Post-plasma-catalytic degradation of toluene using atmosphere double dielectric barrier discharge combined MnO_x-based catalysts >](#)

Shuo Zhang, Jiyan Liang, Xinyang Yu, Tao Xu & Xinjun Shen

Pages: 386-395

Published online: 23 Dec 2019[Graphical abstract](#)

44	0	Altmetric
Views	CrossRef citations	

Article

[Multifunctional lubricant additive derived from polyisobutylene succinimide dispersant >](#)

Shengpei Wang, Shasha Yu, Jianxiang Feng & Shenggao Liu

Pages: 396-406

Published online: 20 Feb 2020

Views CrossRef citations

Article

Synthesis and switchable behavior of a CO₂ responsive polymeric surfactant acting as emulsifier >

Yi Zhao, Yangchuan Ke, Xu Hu, Fangfang Peng, Chengcheng Yu & Liang Xing

Pages: 407-415

Published online: 13 Dec 2019[Graphical abstract](#)

135	0	Altmetric
Views	CrossRef citations	

Article

Effect of organoclay reinforced acrylate latex particles on the cement paste performance >

Farhad Gholinezhad, Mohammad Reza Moghbeli, Amir Aghaei & Ali Allahverdi

Pages: 416-431

Published online: 17 Dec 2019[Graphical abstract](#)

42	0	Altmetric
Views	CrossRef citations	

Article

Apparatus-dependent sol-gel synthesis of TiO₂ nanoparticles for dye-sensitized solar cells >

Jyoti Bansal, Sanjay Kumar Swami, Akanksha Singh, Tarnija Sarao, Viresh Dutta, A. K. Hafiz & Shailesh Narain Sharma

Pages: 432-439

Published online: 23 Dec 2019[Graphical abstract](#)

94	3	Altmetric
Views	CrossRef citations	

Article

Numerical analysis of passive micromixer with novel obstacle design >

Xianchun Shi, Shaofu Huang, Long Wang & Feng Li

Pages: 440-456

Published online: 13 Dec 2019[Graphical abstract](#)

101	1	Altmetric
Views	CrossRef citations	

Article

Kangnan Fan, Zhuji Jin, Xianglong Zhu, Qiulin Wang & Jing Sun

Pages: 457-464

Published online: 11 Dec 2019

101

Views

2

CrossRef citations

Altmetric

Article

Spinel ferrite of MnFe_2O_4 synthesized in *Piper betle* Linn extract media and its application as photocatalysts and antibacterial >

Rahmayeni Rahmayeni, Yenti Oktavia, Yeni Stiadi, Syukri Arief & Zulhadjri Zulhadjri

Pages: 465-474

Published online: 08 Feb 2020[Graphical abstract](#)

69

Views

3

CrossRef citations

Altmetric

Explore

[Most read articles](#)[Most cited articles](#)[Open access articles](#)

Information for

[Authors](#)[Editors](#)[Librarians](#)[Societies](#)

Help and info

[Help & contact](#)[Newsroom](#)[Commercial services](#)[Advertising information](#)[All journals](#)[Books](#)

Open access

[Overview](#)[Open journals](#)[Open Select](#)[Cogent OA](#)[Dove Medical Press](#)[F1000Research](#)[Keep up to date](#)

Register to receive personalised research and resources by email



Sign me up

Copyright © 2021 Informa UK Limited [Privacy policy](#) [Cookies](#) [Terms & conditions](#) [Accessibility](#)Registered in England & Wales No. 3099067
5 Howick Place | London | SW1P 1WG



Spinel ferrite of MnFe_2O_4 synthesized in *Piper betle* Linn extract media and its application as photocatalysts and antibacterial

Rahmayeni Rahmayeni, Yenti Oktavia, Yeni Stiadi, Syukri Arief & Zulhadjri Zulhadjri

To cite this article: Rahmayeni Rahmayeni, Yenti Oktavia, Yeni Stiadi, Syukri Arief & Zulhadjri Zulhadjri (2021) Spinel ferrite of MnFe_2O_4 synthesized in *Piper betle* Linn extract media and its application as photocatalysts and antibacterial, Journal of Dispersion Science and Technology, 42:3, 465-474, DOI: [10.1080/01932691.2020.1721011](https://doi.org/10.1080/01932691.2020.1721011)

To link to this article: <https://doi.org/10.1080/01932691.2020.1721011>



Published online: 08 Feb 2020.



Submit your article to this journal [↗](#)



Article views: 57



View related articles [↗](#)



View Crossmark data [↗](#)



Citing articles: 2 View citing articles [↗](#)



Spinel ferrite of MnFe_2O_4 synthesized in *Piper betle* Linn extract media and its application as photocatalysts and antibacterial

Rahmayeni Rahmayeni, Yenti Oktavia, Yeni Stiadi, Syukri Arief, and Zulhadjri Zulhadjri

Department of Chemistry, Faculty of Mathematics and Natural Sciences, Andalas University, Padang, Indonesia

ABSTRACT

The manganese spinel ferrite (MnFe_2O_4) particles were successfully synthesized via a hydrothermal route in green betel leaf (*Piper betle* Linn) extract media. Morphology, structure, and characteristics of the samples were analyzed by Scanning Electron Microscope (SEM), Transmission Electron Microscope (TEM), X-Ray Diffraction (XRD), Fourier-Transform Infrared (FT-IR), Diffuse Reflectance Spectroscopy UV-Vis (DRS UV-Vis), and Vibration Sample Magnetometer (VSM) instruments. Photocatalytic activity of the spinel ferrite was evaluated by the degradation of dye under solar light and antibacterial activity was studied with different strains of Gram-positive and Gram-negative bacteria. The results revealed that the concentration of betel leaf extract was an important factor, which affects the morphology, crystallization, and magnetic properties of MnFe_2O_4 . The prepared samples exhibited soft-ferromagnetic behavior at room temperature. Un-calcined samples showed higher saturation magnetic (~ 65 emu/g) than calcined samples (29–41 emu/g). The band gap energy of synthesized samples was about 2.05 eV. Two major wide-ranging metal-oxygen (M-O) peaks are seen in the FT-IR spectra in the range of $570\text{--}300\text{ cm}^{-1}$, which confirmed the presence of tetrahedral and octahedral sites in the spinel structure. The MnFe_2O_4 particles showed effective photodegradation for Direct Red 81 dye under solar light irradiation. Moreover, the prepared samples exhibited significant activity as an antibacterial against *Staphylococcus aureus* and *Escherichia coli*.

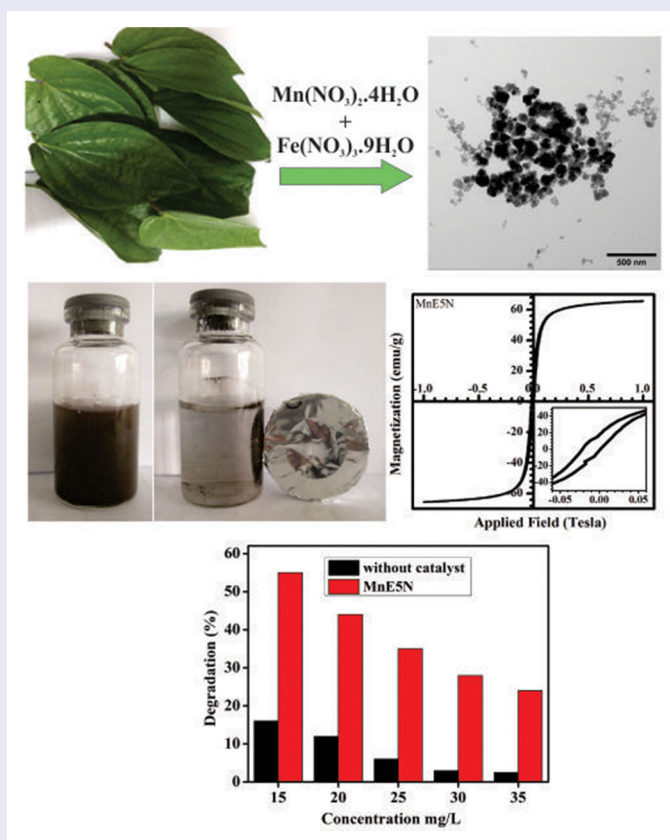
ARTICLE HISTORY

Received 30 October 2019
Accepted 19 January 2020

KEYWORDS

MnFe_2O_4 ; betel leaves; magnetic; Direct Red 81; antibacterial

GRAPHICAL ABSTRACT



Introduction

Magnetic materials are of great interest for both fundamental science and technological applications due to their chemical and physical properties, especially their magnetic properties. Spinel ferrite is a magnetic material that has a narrow band gap ($< 2\text{ eV}$) with the molecular formula AB_2O_4 , where A is a divalent metal ion and B is Fe^{3+} . Spinel ferrite has several spinel structures, including normal, mixed, and inversed spinel. For mixed spinel structures such as MnFe_2O_4 , two sub-lattices at A position (tetrahedral site) and B position (octahedral site) are occupied by Mn^{2+} and Fe^{3+} ions.^[1,2] Recently, spinel ferrite has attracted the attention of researchers and has been widely developed due to its wide and potential applications such as data storage, biosensors, pharmaceutical delivery, disease diagnosis, hyperthermia, gas sensors, electronic devices, energy conversion, magnetic fluid, photocatalysts, antibacterial, and electro communication.^[3–7]

Most of spinel ferrites including MnFe_2O_4 have been used as photocatalysts for environmental remediation such as elimination of azo dyes from wastewater, due to their outstanding properties of nanometer size, excellent optical absorption over low energy photon, chemical stability, large surface area to volume ratio, eco-friendly and high saturation magnetization. The recovery of the magnetic MnFe_2O_4 materials can be done quickly using magnetic fields for the solution after the reaction, providing an attractive and cost-effective method for practical operation. Besides, the MnFe_2O_4 nanoparticles also can be used as an antibacterial which is contained in wastewater because the radicals ($\cdot\text{O}_2^-$, $\cdot\text{OH}$) generated through the redox mechanism reactions during the photocatalytic process can attack the cell membrane components of bacteria and inhibit the growth of these microorganisms.^[1,8]

In a variety of applications, morphology, particle size, and characteristic of manganese ferrite are very important, which depends on the methods, chemical, and reaction path in synthesis. MnFe_2O_4 has been synthesized with various types of methods and then used for many applications. MnFe_2O_4 was synthesized by solvothermal and used for phosphoproteome analysis,^[8–10] by sol-gel process and used as a catalyst for degradation of methylene orange,^[2] and by sol-gel self-combustion technique and its cytotoxicity was evaluated against 4 TI murine breast cancer.^[4] MnFe_2O_4 was also prepared by electrochemical/chemical for electrode,^[11] by thermal decomposition for degradation of phenol in the presence peroxydisulfate,^[12,13] by solution combustion method for antibacterial and photocatalytic process,^[1,9] by microwave and conventional combustion, and by microwave irradiation technique for photocatalytic degradation of methylene blue dye.^[14,15] Each of these methods has its advantages and limitations. However, there was no report about the synthesis of MnFe_2O_4 by a hydrothermal method in natural extract media and applied as a catalyst for Direct Red 81 dye degradation and antibacterial agent.

Numerous of natural extract has been used in synthesis of ferrite such as; *aloe vera* in the synthesis of nanocrystalline MFe_2O_4 ($\text{M} = \text{Cu}, \text{Ni}, \text{Zn}$), *Hibiscus rosa-Sinensis* in

synthesis of CuFe_2O_4 and ZnFe_2O_4 nanoparticles,^[16,17] sesame seeds extract in synthesis of CoFe_2O_4 ,^[18] *Nephelium lappaceum* L in green synthesis CoFe_2O_4 ,^[19] and *moringa oleifera* in synthesis ZnFe_2O_4 .^[20] Green betel leaf extract can be used as a media in synthesizing nanomaterial because it provides a simple, efficient, and green route. Green betel leaves (*Piper betle* Linn) contain many photochemical ingredients such as tannins, flavonoids, alkaloids, terpenoids, saponins, glycosides, and reducing sugars, which expected to act as capping, stabilizing, or reducing agent.^[21] Betel leaf extract has been used as a reducing agent and stabilizer in the synthesis of Fe_2O_3 and silver nanoparticles^[22,23] and stabilizers as well as capping agents in the synthesis of gold nanoparticles.^[24] Punuri et al., in their work about the green synthesis of Au nanoparticle found that polyphenols and flavonoids derived from betel leaf extract can be used as capping agents and stabilizers in the synthesis of nanoparticle materials.^[25]

In this paper, we report the hydrothermally green synthesis of MnFe_2O_4 in the presence of green betel leaf extract. The active compounds contained in betel leaf extract serve as capping agents that capturing the metal ions and regulates the nanostructures of MnFe_2O_4 spinel ferrites. The advantages of this method include the use of inexpensive, nontoxic, and environmentally friendly precursors and simple procedures. The synthesized samples were characterized by several instruments for analyzing the effect of treatment in synthesis on structural, morphological, crystallinity, interaction in molecules, magnetic, and optical properties. Furthermore, the MnFe_2O_4 spinel ferrites were applied as photocatalysts for Direct Red 81 dye degradation and antibacterial agent.

Materials and methods

Materials

Reagents used in the present work were purchased from Merck without further treatment. The materials used in this study are: $\text{Fe}(\text{NO}_3)_3 \cdot 9\text{H}_2\text{O}$ (Aldrich), $\text{Mn}(\text{NO}_3)_2 \cdot 4\text{H}_2\text{O}$ (Aldrich), NaOH, Nutrient agar, and distilled water. Direct Red 81 dye was obtained from the local textile industry, and green betel leaves were taken from the local area of Padang city, Indonesia. The pathogen bacteria were obtained from the Microbiology Laboratory of Agriculture Faculty, Andalas University. All solutions were prepared using deionized water.

Green betel leaf extract preparation

Green betel leaves were dried at room temperature ($28 \pm 2^\circ\text{C}$) and ground to powder. Then 5 grams of fine powder of betel leaves was added 50 mL of distilled water and then was stirred (500 rpm) at 60°C for 2 h. The mixture was cooled, filtered, and then stored in the refrigerator for a while.

Synthesis of MnFe_2O_4 particles

MnFe_2O_4 particles were synthesized through a green synthesis approach using a hydrothermal method in betel leaf

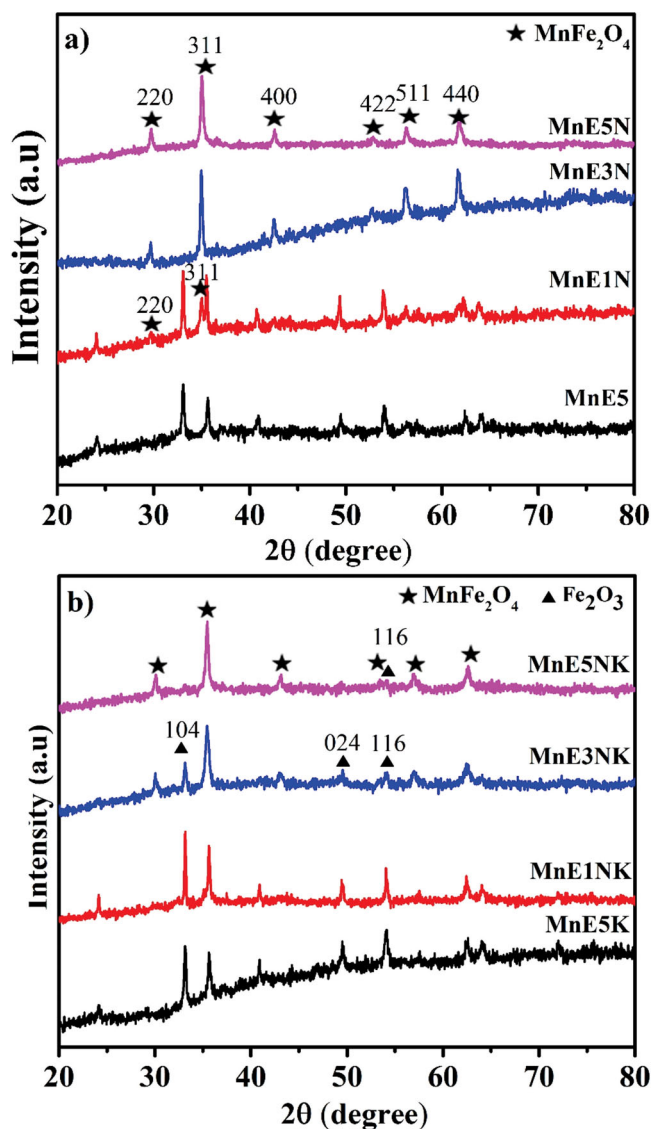


Figure 1. XRD pattern of (a) un-calcined and (b) calcined of MnFe_2O_4 samples.

extract media.^[19] The synthesis of MnFe_2O_4 particles was made as follows: 5 mmol of $\text{Mn}(\text{NO}_3)_2 \cdot 4\text{H}_2\text{O}$ and 10 mmol of $\text{Fe}(\text{NO}_3)_3 \cdot 9\text{H}_2\text{O}$ were dissolved in 50 mL distilled water contain betel leaf extract (45:5). The solution was stirred at 500 rpm for 2 h at room temperature. The mixtures were transferred into an autoclave reactor and heated at 180°C for 2 h. After cooling to room temperature naturally, the blackish-brown produced of MnFe_2O_4 were heated at 110°C for 12 h. The dried product was crushed and then put into a box furnace and calcined at 500°C for 2 h. The formed samples were labeled as MnE5 and MnE5K, respectively for before and after calcination. The other samples were synthesized as the following procedure: 5 mmol of $\text{Mn}(\text{NO}_3)_2 \cdot 4\text{H}_2\text{O}$ and 10 mmol of $\text{Fe}(\text{NO}_3)_3 \cdot 9\text{H}_2\text{O}$ dissolved in 50 mL solution of distilled water contain green betel leaf extract with a volume ratio of 49:1, 47:3, and 45:5 and stirred for 1 h. Under magnetic-stirring (500 rpm), the pH was slowly raised to about 12 by adding sodium hydroxide (NaOH) 4M solution, and stirring was continued for 2 h. After that, the suspension was transferred into an autoclave reactor and heated at 180°C for 3 h. Then, the autoclaves

were cooled at room temperature and the produced precipitates were filtered, rinsed with distilled water to neutral pH, and then dried at 110°C for 4 h. The final powders were labeled as MnE1N, MnE3N, and MnE5N for volume ratio of distilled water to green betel leaf extract were 49:1, 47:3, and 45:5 respectively. The effect of temperature on morphology, structure, and character was studied by calcination MnE1N, MnE3N, and MnE5N samples partially at 500°C for 2 h. Calcined powders were labeled as MnE1NK, MnE3NK, and MnE5NK, respectively.

Characterization of MnFe_2O_4 particles

XRD pattern of MnFe_2O_4 was collected on an XRD (XPERT-PRO diffractometer system) using $\text{Cu K}\alpha$ radiation ($\lambda = 0.15405 \text{ nm}$) at a scanning rate of $10^\circ/\text{min}$. Scanning electron microscopic (SEM) images of MnFe_2O_4 materials were obtained with SEM, JEOL JSM-6360LA electron microscope under high vacuum condition. The transmission electron microscopic (TEM) images were gained on a TEM (FEI Tecnai G2 S-Twin). The compositions of materials were characterized by energy-dispersive X-ray spectroscopy (EDS) (Hitachi, Tokyo, Japan). The band gap energy obtained by Diffuse Reflectance Spectroscopy UV-Vis (DRS UV-Vis, SPEC ORD 210 PLUS-223F1936C). Fourier-transform infrared (FT-IR) spectrum of MnFe_2O_4 was collected on FTIR (Thermo Nicolet iS5) using KBr pellets. The magnetic properties of the prepared samples were measured by using a vibration sample magnetic (VSM) (OXFORD VSM 1.2 H).

Photocatalytic activity

The photocatalytic activity of manganese ferrite was determined by the degradation of Direct Red 81 dye under solar light. The procedure was adopted from the previous study.^[19] The magnetic material of MnE3N, MnE3NK, MnE5N and MnE5NK (20 mg) were added into 30 mL of (35 mg/L) Direct Red 81 solutions. The mixtures immediately irradiated for 2 h under solar light (at 11.00 am–01.00 pm). After that, the aliquots were collected and the absorbance was measured at 530 nm. The degraded of dye was measured by the following relation; degradation percentage = $(C_o - C_t)/C_o \times 100\%$, where C_o is initial absorbance of the dye solution and C_t is the dye solution at a time in h.^[26] The other parameters like dye concentration and irradiation time, were conducted to get the optimal condition.

Antibacterial activity

Antibacterial activity of the samples was screened against pathogen bacteria, i.e. *Staphylococcus aureus* and *Escherichia coli* as following procedure^[10,27]. Nutrient agar (NA) media was prepared by dissolving an amount of agar in distilled water, boiled, and sterilized in an autoclave at 121°C for 20 min, and then cooled until 45°C . Petri dishes for antibacterial assay were sterilized in an autoclave. Bacterial was sub-cultured in 5 mL of sterile distilled water for overnight. A total of 0.1 mL of the bacteria were added to 20 mL of NA

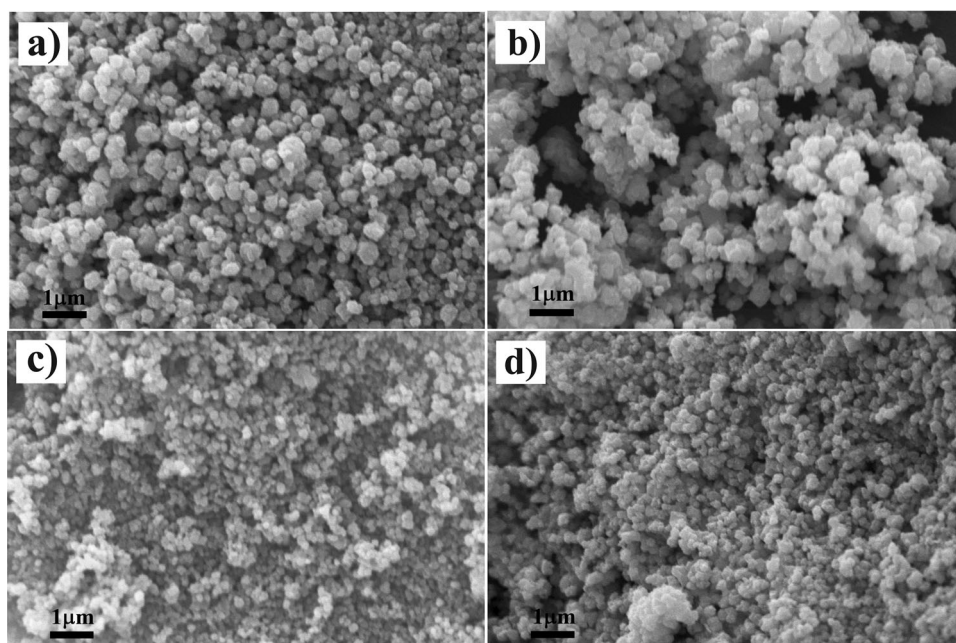


Figure 2. SEM image of (a) MnE3N, (b) MnE3NK, (c) MnE5N, and (d) MnE5NK.

media and homogenized. NA media that already contains the bacteria was poured into a sterile petri dish and allowed to solid. The synthesized MnFe_2O_4 samples were inserted into wells that had been made on the NA media. Amoxicillin as a positive control and water as negative control were also entered into two other wells. The inhibition zone of the samples was measured after incubation at 37°C for 24 h.

Results and discussion

Powder XRD analysis

The structure, phase purity, and crystal size of the spinel MnFe_2O_4 samples were confirmed by analyzing the powder X-ray diffraction (XRD). The crystallographic information obtained by the XRD pattern is displayed in Figure 1. The diffraction pattern in Figure 1(a) shows that the MnE5 sample was forming the MnFe_2O_4 in the amorphous phase with Fe_2O_3 (hematite) as an impurity. While the XRD pattern for the MnE1N sample shows that MnFe_2O_4 has been formed and however, the impurity from Fe_2O_3 still observed. In the XRD pattern of the MnE3N and MnE5N samples, the ferrite manganese peaks are shown by four main peaks that were appeared at $2\theta = 29.72^\circ$, 35.01° , 56.4° , and 62.7° with Miller indices (220), (311), (511), and (440), respectively, which correspond to a cubic structure in the standard of ICSD 155275. There was no impurity of Fe_2O_3 observed. It can be concluded that the amount of betel leaf extract used in synthesis affected the structure of manganese ferrites.

The XRD pattern of the calcined sample of MnE1NK and MnE3NK in Figure 1(b) shows the same peaks with uncalcined samples. The additional peaks of Fe_2O_3 also appeared, which was caused by the breakdown of the unstable manganese spinel ferrite structure due to the rising temperature. The average crystallite size of the samples was

calculated by the Debye-Scherrer equation using the highest intensity diffraction peak of cubic spinel ferrite at the (311) plane.^[28] The average crystallite size of MnE3N, MnE3NK, MnE5N, and MnE5NK were 32.2, 28.8, 19.5, and 28.9 nm, respectively.

Morphological studies

SEM analysis was only carried out for MnE3N, MnE3NK, MnE5N, and MnE5NK samples, as seen in Figure 2(a–d). All the manganese ferrite samples are in a spherical-like shape with almost the same size and pores. The calcined samples (MnE3NK and MnE5NK) have larger particles size than uncalcined (MnE3N and MnE5N). The calcination process of manganese ferrite caused the grain growth of particles, thus give a larger particle size. The MnE5N sample was more homogeneous with a smaller particle size than MnE3N. Whereas for the calcined sample of MnE5NK, the particle size was slightly larger than MnE5N but still smaller than MnE3NK sample. The average particle size of MnE3N, MnE3NK, MnE5N, and MnE5NK were calculated to be around 133, 167, 90, and 120 nm, respectively. The obtained MnFe_2O_4 smaller in particle size and more homogeneous than the sample obtained by the previous studies.^[2,10] These results demonstrated that the concentration of extract and calcination temperature are important factors, which affected the morphology, crystallization, and magnetic properties of MnFe_2O_4 . It was observed from the SEM images that the use of the appropriate amount of betel leaf extract produced fine, homogeneous particles and uniformly dispersed grains. Fine particles estimated due to the presence of secondary metabolites contained in betel leaves acting as ion catchers in solution, which regulates the position of the atoms in the ferrite structure. It is well-known that the homogeneity and particle size are important factors for many purposes of the application.^[29]

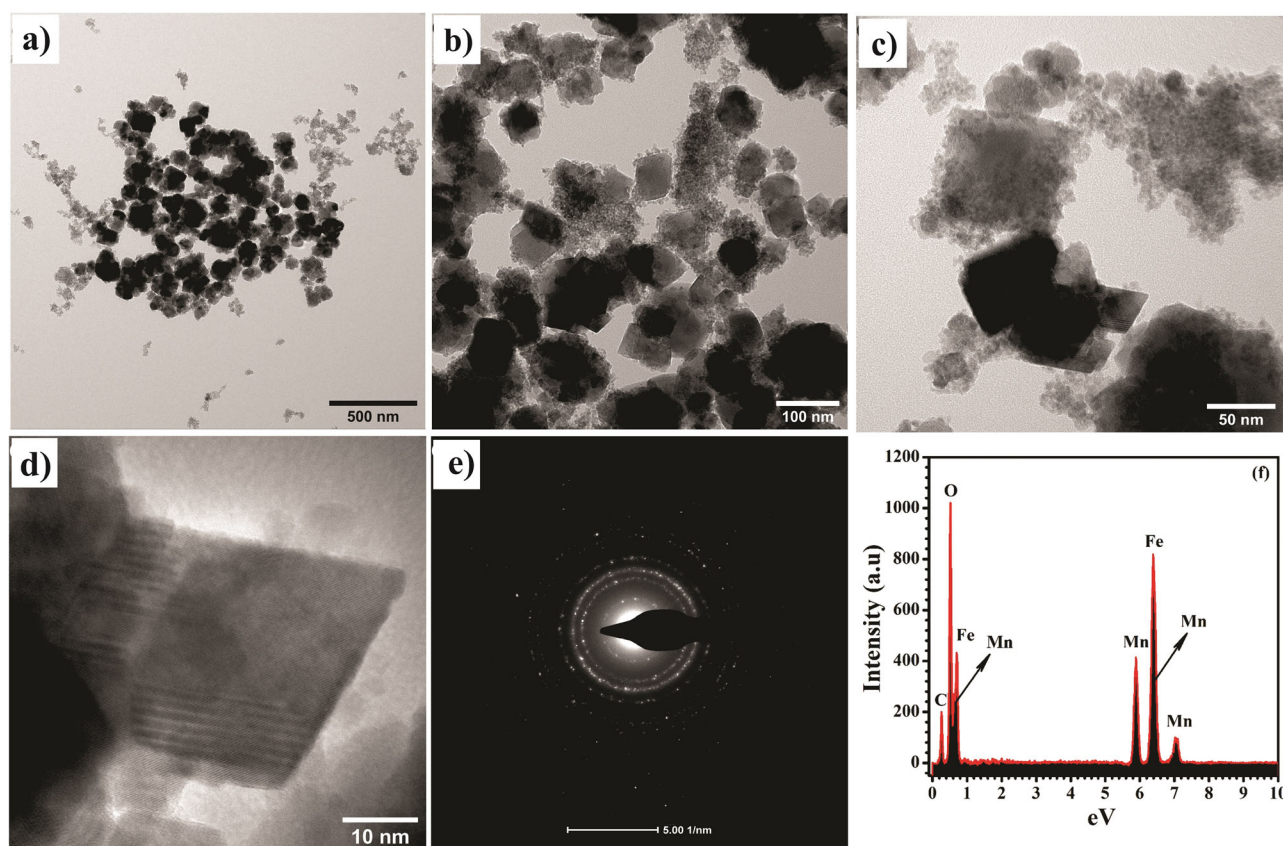


Figure 3. TEM (a-c), HRTEM image (d), SAED pattern (e), and EDX spectra (f) of MnE5N.

More detail analysis of morphology and crystallinity of manganese ferrite can be seen in TEM, and HRTEM images for MnE5N samples were made using 5 mL extract (Figure 3). The standard TEM images (Figure 3a-c) showed that the MnE5N sample was forming the spherical shape, which is a good agreement with the data obtained from SEM images in Figure 2(c). At higher magnification, some particles were observed to be a cube-like shape. The high-resolution transmission electron microscopy (HRTEM) image (Figure 3d) confirms the crystal shape of the cube from the more obvious ferrite manganese with a diameter is about 25 nm, which is slightly larger than the size obtained from XRD analysis. Figure 3e shows the SAED pattern of MnE5N, which confirms the crystalline nature of the final product. EDX analysis, as shown in Figure 3(f) gives the qualitative composition of manganese ferrite of MnE5N nanoparticles. It indicates the presence of Mn, Fe, and O elements in MnE5N samples, which related the MnFe_2O_4 spinel ferrite and established the purity of the sample and no other formation of impurity.

Optical analysis

DRS UV-Vis analysis was carried out to determine the optical properties of nanomaterial. The DRS spectra of manganese ferrites investigated in the range of 200–800 nm. Figure 4a shows the DRS-UV-vis spectra of MnFe_2O_4 particles. All of the samples (MnE3N, MnE3NK, MnE5N, and

MnE5NK) show the absorption peaks at visible area that indicated the optical properties of the samples. The band gap energy was calculated using the following equation, $E_g = 1240/\lambda$, where E_g is band gap energy (eV), h is Plank's constant, c is light velocity, and λ is wavelength (nm).^[30] The band gap energy for MnFe_2O_4 samples was found about 2.05 eV that was close to the MnFe_2O_4 spinel ferrite obtained in the previous study.^[15] It was concluded that the calcination temperature and the extract concentration did not have a significant effect on the changes in the optical properties of the manganese spinel ferrite.

FT-IR analysis

Figure 4(b) shows the FT-IR analysis of MnE3N, MnE5N, MnE3NK, and MnE5NK samples. The two dominant bands were assigned to the metal oxide interaction in spinel ferrite. The strong absorbance bands of MnFe_2O_4 show the Fe-O interaction in tetrahedral site at around $540\text{--}580\text{ cm}^{-1}$. The bands at around $300\text{--}450\text{ cm}^{-1}$ were attributed to the stretching of Mn-O in octahedral site. The spectrum of MnE3N, MnE5N, MnE3NK, and MnE5NK particles was appeared at $401, 396, 373$ and 395 cm^{-1} for tetrahedral position and at $566, 561, 563,$ and 569 cm^{-1} , respectively for octahedral position. The difference in absorption band position was caused by the difference of the M-O bond distance in ferrites. It can be concluded that the temperature

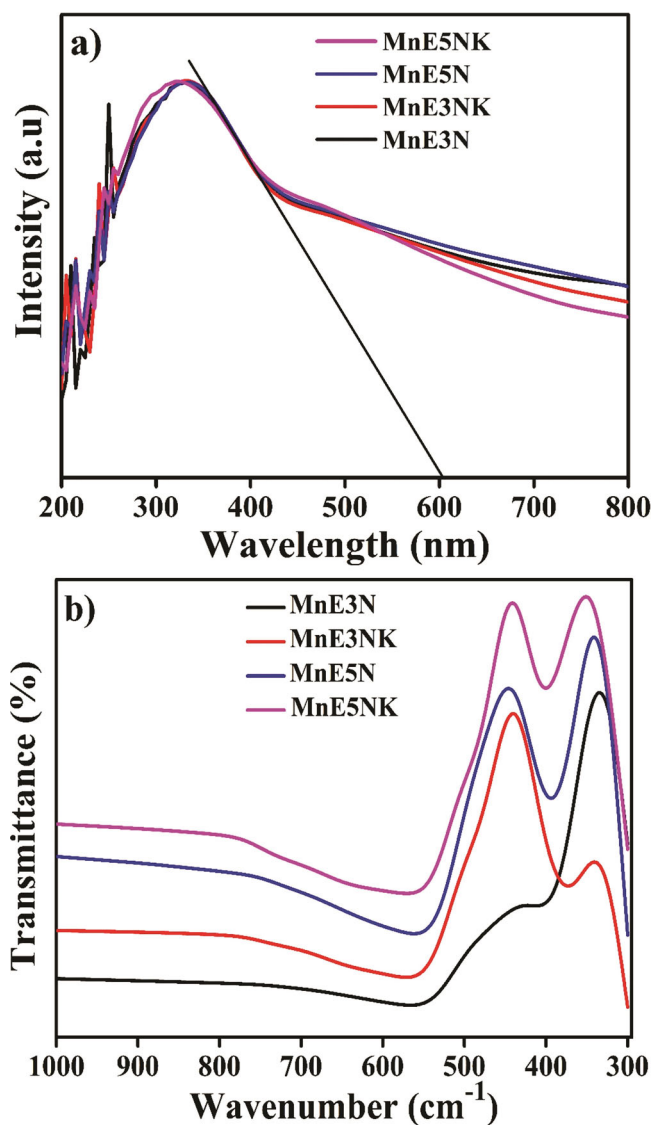


Figure 4. DRS UV-Vis (a) and FT-IR (b) spectra of synthesized manganese ferrites.

and concentration of extract in the synthesis of manganese ferrites affect the structure of MnFe_2O_4 .^[31]

VSM analysis

Figure 5 (a–d) including the insert (magnified views of hysteresis loops at low applied fields) shows the hysteresis loop of the un-calcined and calcined samples, which was measured by VSM. The hysteresis loop is typical for soft ferromagnetic materials for both un-calcined MnE3N and MnE5N samples.

The saturation magnetization (M_s), remanent magnetization (M_r), and coercivity (H_c) value of the samples are shown in Table 1. The M_s value for MnE3N and MnE5N samples are closed to each other, but less than the value obtained by the previous study.^[9] The different in M_r and H_c may be attributed to the internal microstructure in spinel ferrite.^[24,29] The calcined MnE3NK and MnE5NK samples also exhibit soft-ferromagnetic behavior with M_s value lower than un-calcined samples. The coercive value of the calcined

samples was higher than un-calcined; however, for the un-calcined samples have higher saturation magnetic than calcined. It is estimated the calcination process of manganese ferrite causes a change in the dipole direction in the spinel structure which impacts to decreasing of magnetic properties.

Figure 6a shows the MnE5N sample in solution and the separation of the material using a bar magnet (Figure 6b). The magnetic strength behavior of the samples gains profit on the photocatalytic process due to easily separated from solution and used for the next application. The high magnetization properties are important in water treatment applications.

Photocatalytic activity

The photocatalytic activity of manganese ferrite was determined by the degradation of Direct Red 81 dye under solar light irradiation. The degradation percentage of MnE3N, MnE5N, MnE3NK, and MnE5NK after irradiated under solar light for 2 h are 40.6, 56.5, 35.1, and 44.8%, respectively. Figure 7a shows the effect of dye concentration on degradation percentage of Direct Red 81 using MnE5N ferrite as a catalyst and without a catalyst. From the picture can be seen that at the dye concentration of 15 mg/L the degradation percentage reaches 56.5% after 2 h irradiated under the sun (experimental conditions: 20 mg catalyst was dispersed in 30 mL dye solution), whilst without the catalyst only reaches 16%. As the concentration of the dye increases, the degradation percentage of dye decreases due to the increasing number of dye molecules in the solution limits the light penetration to the catalyst material. The reduced penetration of light into the solution causes the reduction in the e-transfer process from the valence band to the conduction band of manganese ferrite so that the formation of $\cdot\text{OH}$ free radicals is reduced. As well known that $\cdot\text{OH}$ radicals are responsible for the degradation of dye molecules into simpler compounds (CO_2 and H_2O).^[32] The effect of irradiation time on the degradation percentage of dye can be seen in Figure 7 (b) (experimental conditions: volume of the dye 30 mL, MNE5N catalyst mass of 20 mg). From the curve, it can be seen that the amount of Direct Red 81 degraded increases with increasing contact time because a greater number of $\cdot\text{OH}$ radicals formed.

The mechanism of the photodegradation process of dye solutions in the presence of MnFe_2O_4 as photocatalysts under solar light is based on the redox reactions. The photodegradation originated when the solar light irradiated on the catalyst. The absorbed photon energy ($h\nu$) either equal to or greater than the energy band gap of MnFe_2O_4 photocatalyst. In the photoexcitation process, the electron in valence bond (VB) moves to conduction band (CB) and leaves h^+ at VB, and then reacts with oxygen from water in order to generate anionic superoxide radical. It takes in the oxidation part and avoids the recombination of e^-/h^+ pair at VB. The protonation of superoxide radicals produced peroxide and then was dissociated forming $\cdot\text{OH}$ radicals. On the other side, h^+ reacts with hydroxy ion at VB to produce reactive species of

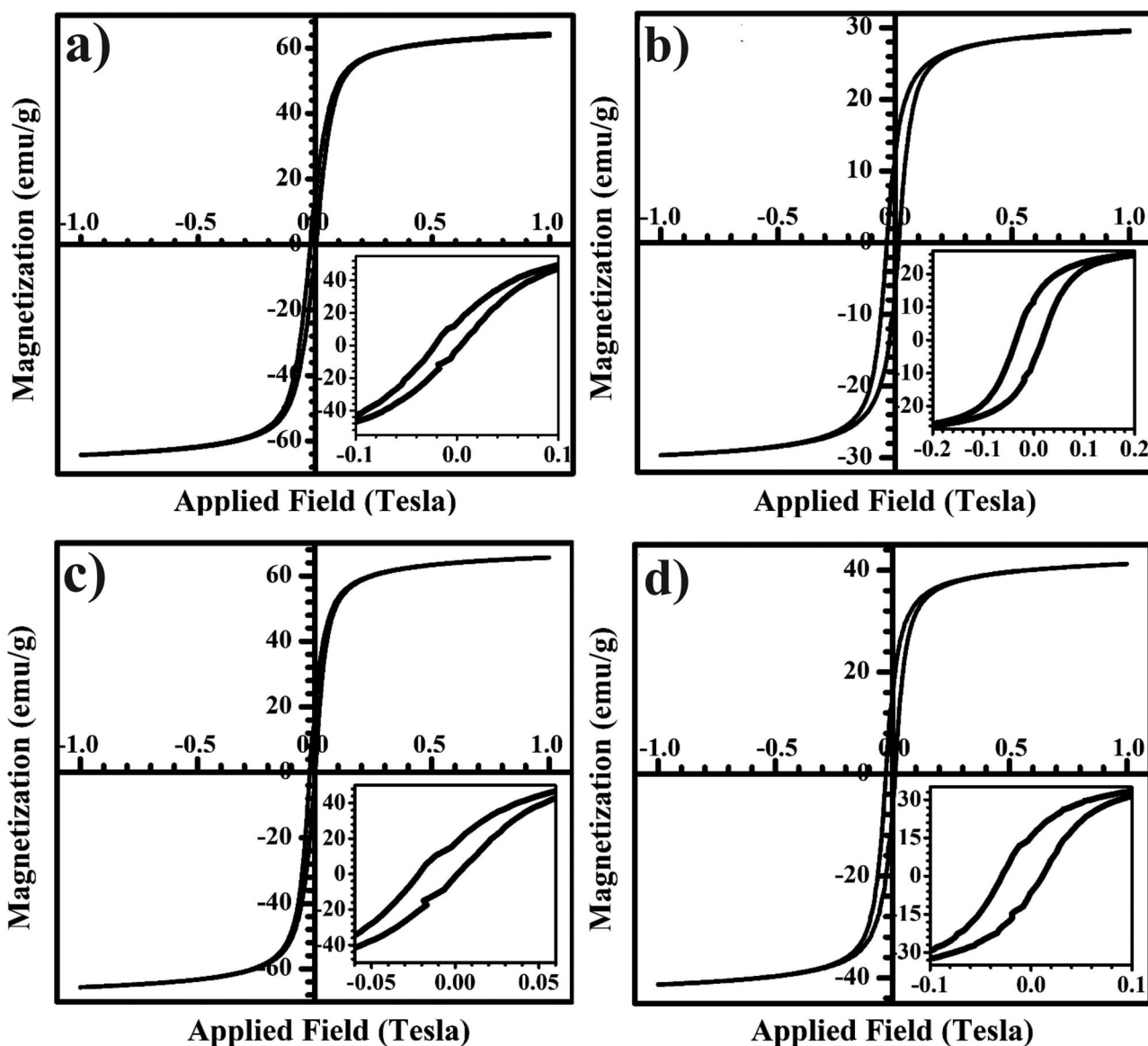


Figure 5. Hysteresis loops of MnE3N (a), MnE3NK (b), MnE5N (c), and MnE5NK (d).

Table 1. The summary of the magnetic properties and photocatalytic activity of the samples.

Sample	(emu/g)		(Tesla)
	Remanent Magnetization	Saturation Magnetization	Coercive Field
MnE3N	13.8068	64.3279	0.0037
MnE3NK	12.1527	29.6591	0.0168
MnE5N	17.2269	65.5866	0.0014
MnE5NK	15.4608	41.2711	0.0114

$\cdot\text{OH}$ radicals which is take in the reduction process part. These reactions occurred on the surface of irradiated MnFe_2O_4 and $\cdot\text{OH}$ radicals produced are a very strong agent which will attack the dye molecules and cause them mineralized to be simpler molecules i.e. CO_2 and H_2O .^[1,33]

Antibacterial activity

The antibacterial activity of manganese ferrite of MnE5N and MnE5NK was performed on gram-positive

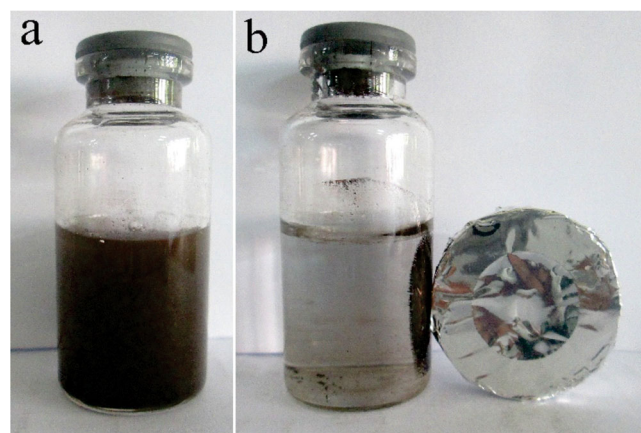


Figure 6. The photos of MnE5N in solution (a) and under the influence of a magnetic field (b).

(*Staphylococcus aureus*) and gram-negative (*Escherichia coli*) bacterial strains. Figure 8 shows the MnE5N and MnE5NK samples have significant antibacterial activity against

Staphylococcus aureus bacteria with an inhibition area of 26.6 mm and 18.9 mm (Figure 8a). This result was higher compared to *Escherichia coli* bacteria with an inhibition area of 4.2 and 6.2 mm for MnE5N and MnE5NK (Figure 8b). The bacterial activity of manganese ferrite depends on the

size, morphology, surface area, chemical molecule diffusion ability and also the discharge of metal ions.^[1] The antibacterial ability of MnE5N samples was better than MnE5NK because of the smaller particle size of MnE5N so that it easily covers and penetrates the cell walls of bacteria. Besides, *Staphylococcus aureus* bacteria are more easily inhibited than *Escherichia coli* due to this bacterial has a structure with high peptidoglycan content so it is difficult to penetrate the cell walls of bacteria and inhibit its growth. Ashwini et al. was synthesized and tested the manganese ferrite antibacterial activity against *Staphylococcus aureus* and *Escherichia coli* but showed no antibacterial activity at all due to the small outer surface of the ferrite material.^[9] According to, Ref.^[34] bactericidal activity would differ depending on the cell wall nature of bacteria. The cell wall of Gram-positive bacteria is wider than the cell the Gram-negative bacteria.^[34] The proposed mechanism of antibacterial activity of the photocatalytic materials are described as followed. When coming in contact with microbes, they will affect the bacterial cell membrane and start to influence the metabolism of the cells. The radical groups generated through the redox mechanism reactions during the photocatalytic process are estimated attack the cell membrane components of bacteria and inhibit the growth of these microorganisms.^[8]

Conclusion

Herein, we have reported the crystallinity, morphology, microstructural, magnetic and optical properties, and activity of manganese ferrites (MnFe_2O_4) synthesized by a green synthesis method in the presence of betel leaf extract as capping agent. The SEM, TEM and HRTEM study demonstrate that the samples are in good homogeneity, nanosized, and crystalline character. The magnetic study shows the samples have soft-ferromagnetic properties. The catalytic activity of the sample reached 56.5% on the degradation of Direct Red 81 dyes after 2 h irradiated under the sun. Manganese ferrite showed significant activity against *Staphylococcus aureus* and *Escherichia coli*.

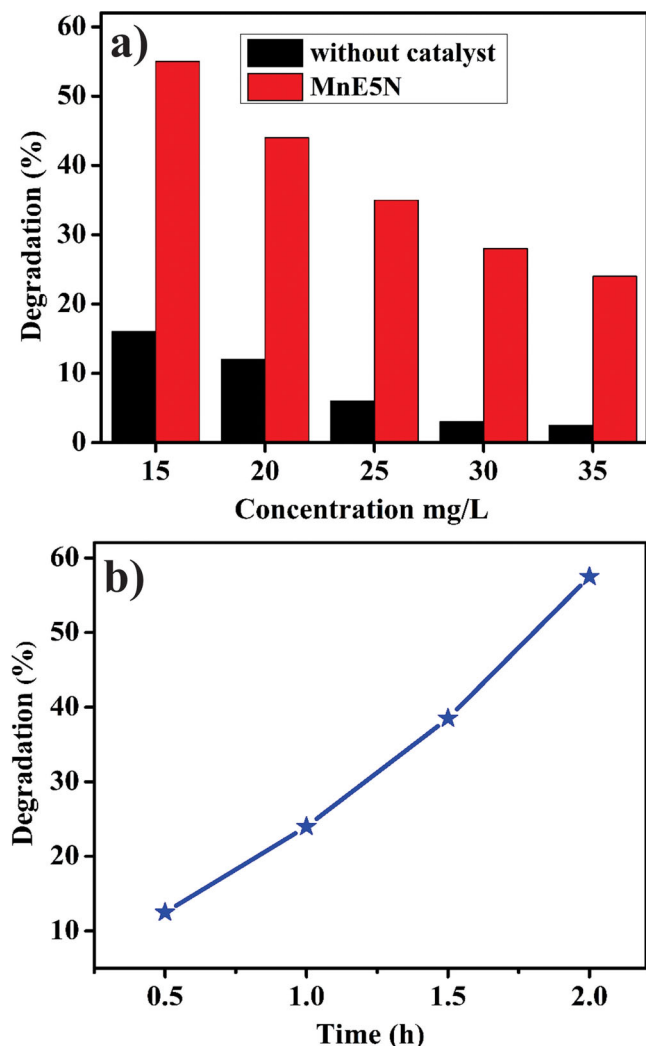


Figure 7. Photocatalytic activity of MnE5N on degradation textile dye of Direct Red 81 with variation of dye concentration (a) and contact time (b).

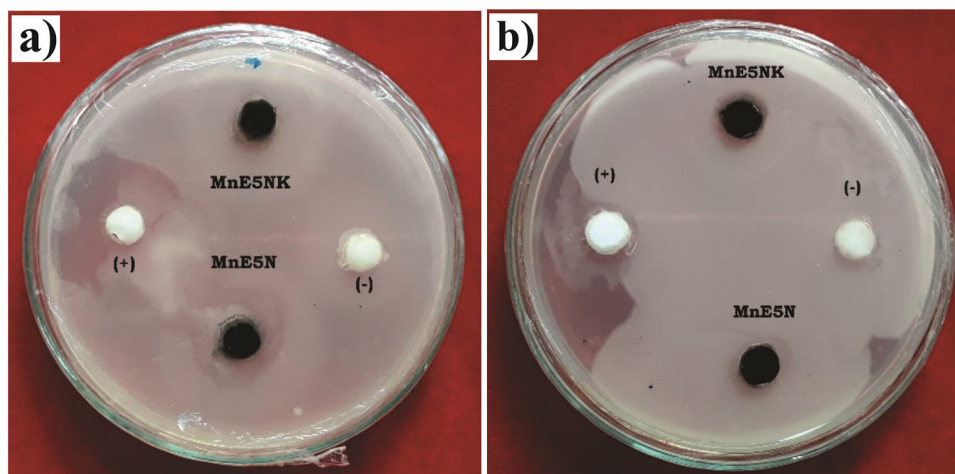


Figure 8. Antibacterial test results of MNE5N and MnE5NK samples against *Staphylococcus aureus* (c) and *Escherichia coli* (d).

Acknowledgments

The authors would like to thank the Directorate General of Higher Education, Ministry of National Education of Indonesia, and LPPM of Andalas University for funding this work through the research grants of Penelitian Dasar Kompetitif program.

Declaration of interest statement

The authors declare no conflict of interest

Funding

This work supported by The Ministry of Research, Technology, and Higher Education of the Republic of Indonesia under Penelitian Dasar Kompetitif grant with contract number: T/24/UN.16.17/PT.01.03/PD-MM/2019.

References

- [1] Madhukara, N. M.; Bhojya, N. H. S.; Nagaraju, G.; Vinuth, M.; Raja, N. H.; Vinu, K. Green Synthesis of Zinc Ferrite Nanoparticles in Limonia Acidissima Juice: Characterization and Their Application as Photocatalytic and Antibacterial Activities. *Microchem. J.* **2019**, *146*, 1227–1235. DOI: [10.1016/j.microc.2019.02.059](#).
- [2] Zhang, L.; Zhang, Y. Wu, Sol-Gel Synthesized Magnetic MnFe_2O_4 Spinel Ferrite Nanoparticles as Novel Catalyst for Oxidative Degradation of Methyl Orange. *J. Nanomater.* **2013**, *2013*, 1–6. DOI: [10.1155/2013/640940](#).
- [3] Kefeni, K. K.; Mamba, B. B.; Titus, A.; Msagati, M. Ferrite Nanoparticles: Synthesis, Characterisation, and Applications in Electronic Device. *Mater. Sci. Eng. B* **2017**, *215*, 37–55. DOI: [10.1016/j.mseb.2016.11.002](#).
- [4] Kanagesan, S.; Aziz, S.; Hashim, M.; Ismail, I.; Tamilselvan, S.; Alitheen, N.; Swamy, M.; Purna Chandra Rao, B. Synthesis, Characterization and in Vitro Evaluation of Manganese Ferrite (MnFe_2O_4) Nanoparticles for Their Biocompatibility with Murine Breast Cancer Cells (4T1). *Molecules* **2016**, *21*, 312. DOI: [10.3390/molecules21030312](#).
- [5] Desai, I.; Nadagouda, M. N.; Elovitz, M.; Mills, M.; Boulanger, B. Synthesis and Characterization of Magnetic Manganese Ferrites. *Mater. Sci. Energy Technol.* **2019**, *2*, 150–160. DOI: [10.1016/j.mset.2019.01.009](#).
- [6] Sam, S.; Nesaraj, A. S. Preparation of MnFe_2O_4 Nanoceramic Particles by Soft Chemical Routes. *Int. J. Appl. Sci. Eng.* **2011**, *9*, 4, 223–239.
- [7] Verma, K. C.; Singh, V. P.; Ramb, M.; Shah, J.; Kotnala, R. K. Structural, Microstructural and Magnetic Properties of NiFe_2O_4 , CoFe_2O_4 and MnFe_2O_4 Nano Ferrite Thin Films. *J. Magn. Mater.* **2011**, *323*, 3271–3275. DOI: [10.1016/j.jmmm.2011.07.029](#).
- [8] Regmi, C.; Joshi, B.; Ray, S. K.; Gyawali, G.; Pandey, R. P. Understanding Mechanism of Photocatalytic Microbial Decontamination of Environmental Wastewater. *Front. Chem.* **2018**, *6*, 1–6. DOI: [10.3389/fchem.2018.00033](#).
- [9] Long, X. Y.; Li, J. Y.; Sheng, D.; Lian, H. Z. Spinel-Type Manganese Ferrite (MnFe_2O_4) Microspheres: A Novel Affinity Probe for Selective and Fast Enrichment of Phosphopeptides. *Talanta* **2017**, *166*, 36–45. DOI: [10.1016/j.talanta.2017.01.025](#).
- [10] Ashwini, K.; Rajanaika, H.; Anantharaju, K. S.; Nagabhushanad, H.; Reddy, P. A.; Shetty, K.; Mahesh, K. R. V. Synthesis and Characterization of as-Formed and Calcined MnFe_2O_4 Nanoparticles: A Comparative Study of Their Antibacterial Activities. *Mater. Today Proceed.* **2017**, *4*, 11902–11909. DOI: [10.1016/j.matpr.2017.09.110](#).
- [11] Yang, L. X.; Wang, F.; Meng, Y. F.; Tang, Q. H.; Liu, Z. Q. Fabrication and Characterization of Manganese Ferrite Nanospheres as a Magnetic Adsorbent of Chromium. *J. Nanomater.* **2013**, *2013*, 1–5. DOI: [10.1155/2013/293464](#).
- [12] Mazario, E.; Mayoral, A.; Salas, E.; Menendez, N.; Herrasti, P.; Marcos, J. S. Synthesis and Characterization of Manganese Ferrite Nanoparticles Obtained by Electrochemical/Chemical Method. *Mater. Design* **2016**, *111*, 646–650. DOI: [10.1016/j.matdes.2016.09.031](#).
- [13] Stoia, M.; Muntean, C.; Militaru, B. MnFe_2O_4 Nanoparticles as New Catalyst for Oxidative Degradation of Phenol by Peroxydisulfate. *J. Environ. Sci.* **2016**, *53*, 269–277. DOI: [10.1016/j.jes.2015.10.035](#).
- [14] Silambarasu, A.; Manikandan, A.; Balakrishnan, K.; Jaganathan, S. K.; Manikandan, E.; Aanand, J. S. Comparative Study of Structural, Morphological, Magneto-Optical and Photo-Catalytic Properties of Magnetically Reusable Spinel MnFe_2O_4 Nanocatalysts. *J. Nanosci. Nanotechnol.* **2018**, *18*, 3523–3531. DOI: [10.1166/jnn.2018.14669](#).
- [15] Mathubala, G.; Manikandan, A.; Antony, S. A.; Ramar, P. Photocatalytic Degradation of Methylene Blue Dye and Magneto-optical Studies of Magnetically Recyclable Spinel $\text{Ni}_x\text{Mn}_{1-x}\text{Fe}_2\text{O}_4$ ($x = 1/4, 0.0, 0.5, 1.0$) Nanoparticles. *J. Mol. Struct.* **2016**, *1113*, 79–87. DOI: [10.1016/j.molstruc.2016.02.032](#).
- [16] Kombaiah, K.; Vijaya, J. J.; Kennedy, L. J.; Bououdina, M. Studies on the Microwave Assisted and Conventional Combustion Synthesis of Hibiscus Rosa-Sinensis Plant Extract Based ZnFe_2O_4 Nanoparticles and Their Optical and Magnetic Properties. *Ceram. Int.* **2015**, *42*, 2741–2749. DOI: [10.1016/j.ceramint.2015.11.003](#).
- [17] Manikandan, A.; Durka, M.; Antony, S. A. Hibiscus rosa-Sinensis Leaf Extracted Green Methods, Magneto-Optical and Catalytic Properties of Spinel CuFe_2O_4 Nano and Microstructures. *J. Inorg. Organomet. Polym.* **2015**, *25*, 1019–1031. DOI: [10.1007/s10904-015-0203-8](#).
- [18] Gingasu, D.; Mindru, I.; Mocioiu, O. C.; Preda, S.; Stanica, N.; Patron, L.; Ianculescu, A.; Oprea, O.; Nita, S.; Paraschiv, I.; et al. Synthesis of Nanocrystalline Cobalt Ferrite through Soft Chemistry Methods: A Green Chemistry Approach Using Sesame Seed Extract. *Mater. Chem. Phys.* **2016**, *182*, 219–230. DOI: [10.1016/j.matchemphys.2016.07.026](#).
- [19] Rahmayeni, Alfina, A.; Stiadi, Y.; Lee, H. J. Zuhadjri, Green Synthesis and Characterization of $\text{ZnO-CoFe}_2\text{O}_4$ Semiconductor Photocatalysts Prepared Using Rambutan (*Nephelium Lappaceum* L.) Peel Extract. *Mater. Res.* **2019**, *22*, 1–10. DOI: [10.1590/1980-5373-mr-2019-0228](#).
- [20] Matinise, N.; Kaviyarasu, K.; Mongwaketsi, N.; Khamlich, S.; Kotsedi, L.; Mayedwa, N.; Maaza, M. Green Synthesis of Novel Zinc Iron Oxide (ZnFe_2O_4) Nanocomposite via *Moringa Oleifera* Natural Extract for Electrochemical Applications. *Appl. Surf. Sci.* **2018**, *446*, 66–73. DOI: [10.1016/j.apsusc.2018.02.187](#).
- [21] Kumari, O. S.; Rao, N. B. Phyto Chemical Analysis of Piper Betel Leaf Extract. *World J. Pharm. Pharm. Sci.* **2015**, *4*, 699–703. DOI: [10.1016/j.apsusc.2018.02.187](#).
- [22] Chanu, T. S.; Devi, K. N. Green Synthesis of Fe_2O_3 Nanoparticles Using Piper Betle Leaf and Its Characterization. *IOSR J. Appl. Phys. (IOSR-JAP)* **2018**, *10*, 32–38. DOI: [10.9790/4861-1005033238](#).
- [23] Ramachandran, K.; Kalpana, D.; Sathiskumar, Y.; Lee, Y. S.; Ravichandran, K.; Kumar, G. G. A Facile Green Synthesis of Silver Nanoparticles Using Piper Betle Biomass and Its Catalytic Activity toward Sensitive and Selective Nitrite Detection. *J. Ind. Eng. Chem.* **2015**, *35*, 29–35. DOI: [10.1016/j.jiec.2015.10.033](#).
- [24] Rani, P. U.; Rajasekharreddy, P. Green Synthesis of Silver-Protein (Core-Shell) Nanoparticles Using Piper Betle L. Extract and Its Ecotoxicological Studies on *Daphnia Magna*. *Coll. Surf. A. Physicochem. Eng. Aspects* **2011**, *389*, 188–194. DOI: [10.1016/j.colsurfa.2011.08.028](#).

- [25] Punuri, J. B.; Sharma, P.; Sibyala, S.; Tamuli, R.; Bora, U. Piper Betle-Mediated Green Synthesis of Biocompatible Gold Nanoparticles. *Int. Nano Lett.* **2012**, 2, 1–9. DOI: [10.1186/2228-5326-2-18](https://doi.org/10.1186/2228-5326-2-18).
- [26] Rahmayeni, R.; Arief, S.; Jamarun, N.; Emriadi, E.; Stiadi, Y. Magnetically Separable ZnO-MnFe₂O₄ Nanocomposites Synthesized in Organic-Free Media for Dye Degradation under Natural Sunlight. *Orient. J. Chem.* **2017**, 33, 2758–2765. DOI: [10.13005/ojc/330608](https://doi.org/10.13005/ojc/330608).
- [27] Labanni, A.; Zulhadjri, Z.; Handayani, D.; Ohya, Y.; Syukri, A. The Effect of Monoethanolamine as Stabilizing Agent in *Uncaria Gambir* Roxb. Mediated Synthesis of Silver Nanoparticles and Its Antibacterial Activity. *J. Dispers. Sci. Technol.* **2019**, 41, 1–8. DOI: [10.1080/01932691.2019.1626249](https://doi.org/10.1080/01932691.2019.1626249).
- [28] Pui, A.; Gherca, D.; Cornei, N. Synthesis and Characterization of MFe₂O₄ (M = Mg, Mn, Ni) Nanoparticles. *Mater. Res. Bull.* **2013**, 48, 1357–1362. DOI: [10.1016/j.materresbull.2012.11.088](https://doi.org/10.1016/j.materresbull.2012.11.088).
- [29] Wang, Y. Q.; Cheng, R. M.; Wen, Z.; Zhao, L. J. Synthesis and Characterization of Single-Crystalline MnFe₂O₄ Ferrite Nanocrystals and Their Possible Application in Water Treatment. *Eur. J. Inorg. Chem.* **2011**, 2011, 2942–2947. DOI: [10.1002/ejic.201100205](https://doi.org/10.1002/ejic.201100205).
- [30] Casbeer, E.; Sharma, V. K.; Li, X. Z. Synthesis and Photocatalytic Activity of Ferrites under Visible Light: A Review. *Sep. Purif. Technol.* **2012**, 87, 1–14. DOI: [10.1016/j.seppur.2011.11.034](https://doi.org/10.1016/j.seppur.2011.11.034).
- [31] Phadatare, M. R.; Salunkhe, A. B.; Khot, V. M.; Sathish, C. I.; Dhawale, D. S.; Pawar, S. H. Thermodynamic, Structural, and Magnetic Studies of NiFe₂O₄ Nanoparticles Prepared by Combustion Method: Effect of Fuel. *J. Alloys Compd.* **2013**, 546, 314–319. DOI: [10.1016/j.jallcom.2012.08.092](https://doi.org/10.1016/j.jallcom.2012.08.092).
- [32] Meena, S.; Renuka, L.; Anantharaju, K. S.; Vidya, Y. S.; Nagaswarupa, H. P.; Prashantha, S. C.; Nagabhushana, H. Optical, Electrochemical and Photocatalytic Properties of Sun Light Driven Cu Doped Manganese Ferrite Synthesized by Solution Combustion Synthesis. *Mater. Today Proceed.* **2017**, 4, 11773–11781. DOI: [10.1016/j.matpr.2017.09.094](https://doi.org/10.1016/j.matpr.2017.09.094).
- [33] Patil, S. B.; Naik, H. S. B.; Nagaraju, G.; Viswanath, R.; Rashmi, S. K.; Kumar, V. M. Sugarcane Juice Mediated Eco-Friendly Synthesis of Visible Light Active Zinc Ferrite Nanoparticles: Application to Degradation of Mixed Dyes and Antibacterial Activities. *Mater. Chem. Phys.* **2018**, 212, 351–362. DOI: [10.1016/j.matchemphys.2018.03.038](https://doi.org/10.1016/j.matchemphys.2018.03.038).
- [34] Sathiyavimala, S.; Vasantharajb, S.; Bharathia, D.; Saravananb, M.; Manikandan, E.; Kumard, S. S.; Pugazhendhie, A. Biogenesis of Copper Oxide Nanoparticles (CuONPs) Using *Sida Acuta* and Their Incorporation over Cotton Fabrics to Prevent the Pathogenicity of Gram Negative and Gram Positive Bacteria. *J. Photochem. Photobiol. B Biol.* **2018**, 188, 126–134. DOI: [10.1016/j.jphotobiol.2018.09.014](https://doi.org/10.1016/j.jphotobiol.2018.09.014).